Research Article Open Access

Lijun Lin* and Wei Lin

Study on the response characteristics of oil wells after deep profile control in low permeability fractured reservoirs

https://doi.org/10.1515/phys-2018-0104
Received August 1, 2018; accepted October 27, 2018

Abstract: The rhombus inverted nine-spot well pattern is often adopted in low permeability oilfield development, which has the advantage of high oil production rate and flexible adjustment. Due to the strong heterogeneity of the low permeability reservoirs, the oil wells along the fracture direction are heavily water-flooded and the water cut rises quickly, and the oil wells on both sides of fractures have no response to water injection. Hence, deep profile control is an effective way to solve this kind of plane contradiction, and is widely applied in the low permeability oilfield development. However, because of the asymmetry of the rhombus inverted nine-spot well pattern and the heterogeneity of the low permeability reservoirs, there are differences in the response characteristics of oil wells at different locations after deep profile control. In this paper, combined with physical experiments and numerical simulations, we analyzed oil increment, the distribution of streamlines and slugs of wells at different locations before and after deep profile control, and evaluated the response characteristics of oil wells of rhombus inverted nine-spot well pattern after deep profile control in low permeability fractured reservoirs. It is concluded that the effect of increasing oil production of the side wells is better than that of the angle wells after deep profile control, and the response sequence is side well, angle well in short axis, and angle well in long axis, which is also verified by the practical results of deep profile control in Daqing Oilfield.

Keywords: Low permeability fractured reservoirs; Rhombus inverted nine-spot well pattern; Deep profile control; Physical experiment and Numerical simulation; Response characteristics

PACS: 91.25.Za, 91.60.Ba, 91.60.Np, 91.60.Tn, 91.65

1 Introduction

The development of low permeability fractured reservoirs using the rhombus inverted nine-spot well pattern is often confronted with the problem of uneven water flooding [1–3]. The general performance of water flooding is that the injected water flows along the fracture direction, and the water cuts of corresponding oil wells on fractures rise quickly, such that the water cuts of oil wells and effect of water flooding are apparently controlled by the fracture direction [4–7]. Once the fractures open, the injection pressure of the water well will be reduced, and the water absorption capacity of the reservoir will be enhanced and the ineffective circulation of water injection will become serious [8–10]. Deep profile control is an effective method to solve this kind of plane contradiction, and is widely applied in the low permeability oilfield development [11]. However, due to the asymmetry of the rhombus inverted nine-spot well pattern and the heterogeneity of the low permeability fractured reservoirs, there are significant differences in the response characteristics of oil wells at different locations after deep profile control [12]. In the process of oil and gas development, the macroscopic phenomenon is often the appearance, but the law of oil and gas seepage is the fundamental [13–17]. Therefore, it is of great significance to analyze the response characteristics of the rhombus inverted nine-spot well pattern by using the seepage mechanics method, in order to improve the effect of deep profile control. Nevertheless, at present, there are few researches on the percolation mechanism of deep profile control in the rhombus inverted nine-spot well pattern, and most of them are mainly focused on the timing of water breakthrough [18], the sweep coefficient of water

***Corresponding Author: Lijun Lin:** Shandong Agriculture and Engineering University, Jinan 250100, P. R. China,
E-mail: saeulinlijun@163.com

Wei Lin: University of Chinese Academy of Sciences, Beijing 100049, P. R. China
Institute of Porous Flow and Fluid Mechanics, Chinese Academy of Sciences, Langfang 065007, P.R. China
Research Institute of Petroleum Exploration & Development, Beijing 100083, P. R. China, E-mail: linwei15@mails.ucas.edu.cns

injection [19], and the calculation of fracturing productivity [20, 21]. Furthermore, because the deep profile control is mostly applied to heterogeneous formations with severe injection water channeling, conventional research method of seepage mechanics often fails to analyze the percolation mechanism of deep profile control in the rhombus inverted nine-spot well pattern.

Scholars from all over the world have tried to find out the reasons for the differences in the response characteristics of oil wells at different locations after deep profile control through the method of seepage simulation. Dawe [22] and Liang [23] studied the principle of deep profile control by using micro model and Berea sandstone core experiment, respectively. It was considered that the fundamental reason for the difference in permeability between oil and water after plugging is the separation of oil-water flow channels. Seright [24] used tracer technology to study the effects of permeability, water injection rate after plugging, lithology, and gel properties on the plugging performance of the plugging agent. It found that strong gel can reduce the plugging rate of Berea core with different permeabilities to the same value. For weak gel, the higher the permeability is, the greater the plugging rate is; the residual resistance coefficient after plugging decreases with the increase of water injection speed. Fan [25] and Li [26] employed streamline numerical simulator to analyze the distribution characteristics of streamlines before and after deep profile control, and qualitatively explained the effect of deep profile control on streamlines. In addition, from different perspectives Islam, Rossen and Balan, et al. [27–31] have also proposed several numerical simulation methods such as empirical / semi-empirical model, total balance model, percolation model, and diversion model to simulate the seepage of deep profile control. But there is a lack of targeted research on the rhombus inverted nine-spot well pattern. Furthermore, there is no detailed discussion on the response characteristics and production dynamic change laws of oil wells at different locations (angle wells and side wells) in rhombus inverted nine-spot well pattern after deep profile control.

In this paper, a two-dimensional heterogeneous cementation model was used to study the variation of oil production and water cut of oil wells at different locations of rhombus inverted nine-spot well pattern after deep profile control, and the response characteristics of reducing water production and increasing oil production of oil wells at different locations were also analyzed based on the physical model. In addition, by establishing the numerical simulation model of rhombus inverted nine-spot well pattern considering ground stress, the oil increment, and the variation law of streamline field before and after deep profile control were studied. The response characteristics of different wells in the rhombus inverted nine-spot well pattern were also obtained.

2 Materials and methods

2.1 Physical simulation experiment

2.1.1 Model preparation and experimental fluid

In order to characterize the percolation characteristics of low permeability fractured reservoirs, a heterogeneous flat cementation model was adopted, which was made of epoxy resin and quartz sand. In the model, a high permeability strip was added to the long-axis injection-production well direction to characterize the direction of fracture development. Nine wells were arranged in the model, where I1 is the injection well (water well), P1- P8 are the production wells (oil wells P1 and P5 are the angle wells in the long axis, P3 and P7 are the angle wells in the short axis, and P2, P4, P6, and P8 are the side wells), and the layout of specific well locations are shown in Figure 1. The model size is 0.4 m × 0.3 m × 0.03 m, the average porosity of this model is 13.1%, the matrix permeability is 0.69×10^{-3} um^2, and the permeability in high permeability area is about 200×10^{-3} um^2.

The experimental fluids include the crude oil with viscosity of 30 mpa·s, water with viscosity of 0.5 mpa·s, and gel plugging agent. Gel plugging agent is composed of Polyacrylamide (PAM) with concentration of 0.9% and Phenolic resin crosslinking agent with concentration of 1.0% [32–34]. The performance evaluation indicators of gel plugging agents are shown in Table 1.

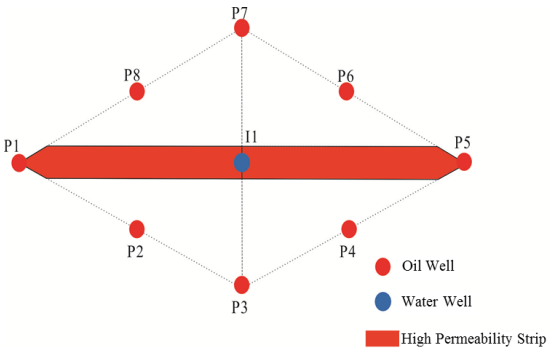

Figure 1: Sketch map of well location

Table 1: Performance evaluation index of gel plugging agent

Viscosity (mPa·s)	Gelation time (h)	Molecular Weight of PAM	Residual resistance factor	Inaccessible pore volume	Maximum adsorption capacity (kg/kg)
20	48	6000000	170	0.15	0.00012

2.1.2 Experimental device and process

The physical simulation experimental device mainly consists of ISCO pump, drug tank, flat cementation core, and output-end oil-water metering device, as shown in Figure 2. The ISCO pump and the drug tank are connected to the water well, which are used for water injection and plugging agent injection, respectively. Each oil well is connected with an oil-water metering device for recording fluid production and water cut change in different wells.

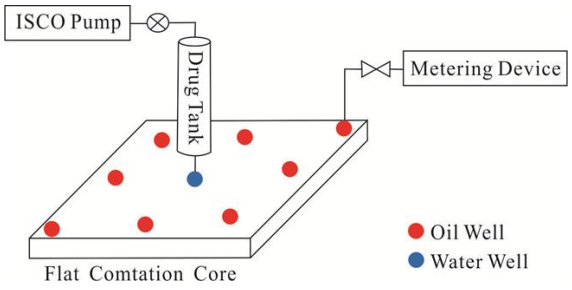

Figure 2: Physical simulation experimental device

In order to simulate the actual reservoir development process, the oil wells in mainstreams (i.e. P1 and P5) were flooded first and had a water content of 98%, which is to simulate the process of water channeling in water injection development. Then the plugging agent was injected into the water well, simulating the deep profile control of the injection well [35]. The specific experimental steps are as follows:

1) First, the model was saturated with water. Then, the crude oil was injected to saturate the model. Finally the model was aged for 7 days.

2) The second water injection was carried out until the water content of the two oil wells (i.e. P1 and P5) reached 98%, and the liquid production and water content data of different oil wells were recorded.

3) The plugging agent was injected into water well.

4) The water injection was repeated to simulate the subsequent water-flooding stage and recorded the fluid production and water cut-off data of the wells at different positions.

2.2 Numerical simulation

2.2.1 Numerical simulation model for deep profile control

According to the physical model shown in Figure 1, a numerical simulation model as shown in Figure 3 is established [36, 37]. In Figure 3, I1 is the injection well, and p1- p8 is the production well. A horizontal fracture runs through P1, I1 and P5. Parameters of geology, fluid, and well pattern are found in Table 2.

3 Results and discussion

3.1 Physical experiment data

The oil productions and the oil increments of 8 production wells at different locations were recorded and calculated, respectively. The specific parameters of oil production are shown in the Table **??**.

Table 3 shows that the two angle wells (P1 and P5) located on the mainstreams have the smallest single-well increase in oil production, and have an average oil increment of 0.85 cm^3. The single-well oil increment of two angle wells (P3 and P7) perpendicular to the high permeability strip is significantly higher than those of P1 and P5, whose average oil increment is 1.3 cm^3. And the single-well oil increase of four side wells (P2, P4, P6, and P8) is the largest, whose average oil increase reaches 4.48 cm^3.

3.2 Numerical simulation analysis

During the development of rhombus inverted nine-spot well pattern, serious flooding occurs along the direction of principal stress and is not effective in the direction of vertical principal stress. The shape of streamline before and after profile control is analyzed by means of numerical simulation, as shown in Figure 3. Before deep profile control, because the conductivity of the fracture is higher

Table 2: Parameter list of numerical model

Parameters	Value	Parameters	Value
Permeability ($10^{-3}\mu m^2$)	0.69	Saturation pressure (MPa)	6.91
Porosity (%)	13.1	Formation volume factor	1.206
Oil viscosity (mPa·s)	30	Well pattern	rhombus inverted nine-spot well pattern
Formation pressure (MPa)	9.79	Grid number	200×150×15
Grid spacing (m)	0.002×0.002×0.002	Development direction of fracture	the direction is parallel to the long axis
Fracture permeability ($10^{-3}\mu m^2$)	200		

Table 3: Statistical data of oil increment in single well

Well number	Oil production before deep profile control (cm^3)	Oil production after deep profile control (cm^3)	Oil increment (cm^3)
P1	8.9	9.7	0.8
P2	2.2	6.6	4.4
P3	4.5	5.7	1.2
P4	2.3	6.7	4.4
P5	8.6	9.5	0.9
P6	2.2	6.7	4.5
P7	4.4	5.8	1.4
P8	2.3	6.9	4.6

than that of the matrix, the streamlines are dense along the fracture direction (I1 - P1, I1 - P5), and the streamlines along the vertical fracture direction are relatively sparse. A large amount of injected water flows along the fracture direction, resulting in rapid flooding of the angle wells (P1, P5).

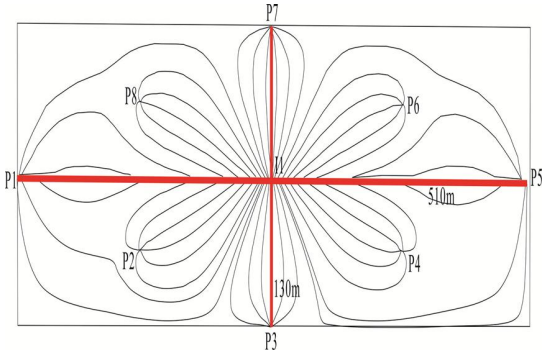

Figure 3: Streamline distribution before deep profile control of rhombus inverted nine-spot well pattern

Plugging measures are conducted to the injection well I1, and the distribution of streamlines after plugging is shown in Figure 4. As can be seen from Figure 4, the plugging agent forms a block plug along the direction of the fracture, which indicates that the plugging agent mainly seepage along the fracture zone (i.e. I1 - P1, I1 - P5). After plugging, the injected water needs to bypass the plugging section and sweep outward, and there is no streamline through the slug area, thus enlarging the sweep area of injection water between the side wells (P2, P4, P6, and P8) and the angle well (P3, P7), and displacing the dead oil in this area in large quantities.

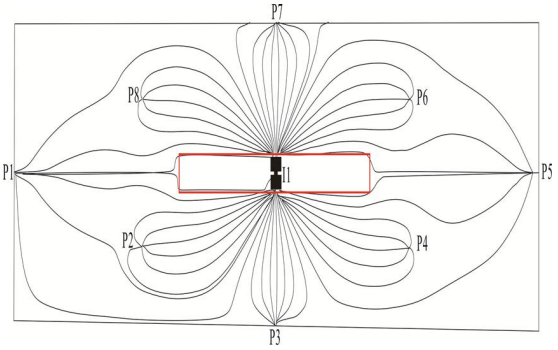

Figure 4: Diagram of streamline and slug distribution after deep profile control of rhombus inverted nine-spot well pattern

Based on the results of numerical simulation, the field data of accumulated oil production before and after deep profile control are first derived. Then, the two oil increment data before and after profile control of each grid are subtracted into excel to calculate, so the oil increment data of each grid are obtained. Finally, the field data of the oil increment is introduced into eclipse, and the distribution field of the oil increase after the deep profile control is obtained, as shown in Figure 5. It can be concluded from Figure 5 that the oil increasing area is mainly concentrated in the area between the side wells (P2, P4, P6, and P8) and the angle well (P3, P7), but the effect of increasing oil production is not obvious for the area near the angle wells along fracture direction (P1, P5). The results of the numerical simulation coincide with the physical experiment data well.

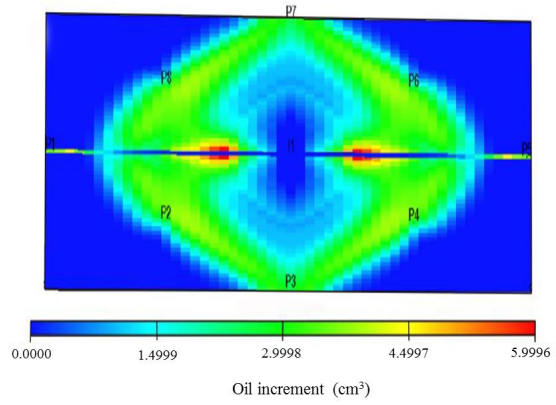

Figure 5: Field diagram of oil increment distribution after deep profile control of rhombus inverted nine-spot well pattern

4 Case verification

Daqing Oilfield (Dq) employs the rhombus inverted nine-spot well pattern of 150 m × 500 m to develop, and has the formation permeability of 0.67×10^{-3} μm^2, the average effective porosity is 10.14%. The reservoir plane permeability difference is great, and the heterogeneity is strong. Dq Oilfield has the current oil recovery factor of 10.4% and the total water cut of 57%, and has a clear direction of horizontal water channeling. From 2008 to 2012, the deep profile control was carried out in Dq Oilfield. The oil increase after the profile control is counted and the results are shown in Table 4.

According to the oil increment effect of deep profile control on actual block (Table 4), it can be seen that after the deep profile control in rhombus inverted nine-spot well pattern, the oil increment of most long-axis angle wells is 0, and only two of them have less than 10 tons of oil increment, which is significantly less than the oil increase of the side wells and the angle wells in short axis. The increase in oil production of side wells is the highest and exceeds 100 t. The effect of deep profile control in real blocks is consistent with the characteristics described in the previous physical model and mathematical model.

5 Conclusions

In this paper, taking the actual block as an example, the heterogeneous cementation physical model and the numerical simulation model of streamline are established. By analyzing the oil increment and distribution characteristics of streamline before and after profile control, it is considered that the streamlines do not pass through the plugging area and spread outward through bypassing the plugging slug, which results in the increase in the swept coefficient of water flooding and the reduction of dead oil area. By comparing and analyzing the oil increasing field before and after deep profile control, the oil increasing area of deep profile control in rhombus inverted nine-spot well pattern is mainly concentrated in the area between the side wells and the short-axis angle wells. However, there is no obvious oil increasing effect in the area near the long-axis angle wells. Moreover, the results of the physical experiment and the numerical simulation agree well with the actual oil field production. Therefore, it is suggested that side wells and angle wells should be arranged in the remaining oil enrichment area in the later period of well pattern adjustment, the oil recovery thus can be improved to the maximum.

Acknowledgement: We gratefully acknowledge the financial supports from Shandong Provincial Natural Science Foundation, China(ZR2018BA024), the National Science and Technology Major Project (2017ZX05013-001) and the Project of Shandong Province Higher Educational Science and Technology Program (No. J17KB069).

Conflicts of Interest: The authors declare no conflict of interest.

Table 4: The effect of deep profile control in Dq Oilfield

Well group number	Oil increment of angle well in long axis (t)	Oil increment of angle well in short axis (t)	Oil increment of side well (t)
P34-21	0	105	398
P34-27	0	118	258
P34-31	7	49	443
P40-25	0	57	142
P73-08	0	26	119
X32-12	0	34	138
X34-15	0	16	109
X24-110	2	69	587
X24-108	0	47	121

References

[1] Mingqiang H., Yongle H., Xiangui L., An overview on characteristics of low-permeability fractured reservoirs, Special Oil & Gas Reservoirs, 2007, 14(3), 12-15.

[2] Chunsheng P., Cheng J., Yanlong H., et al., Multistage interwell chemical tracing for step-by-step profile control of water channeling and flooding of fractured ultra-low permeability reservoirs, Petrol. Explor. Develop., 2016, 43(4), 679-688.

[3] Ming W., Weiyao Z., Jishan L., et al., Two-phase percolation of rhombus inverted nine-spot fracturing well pattern in low permeability oil reservoirs, Rock & Soil Mechanics, 2010, 31(10), 3295-3299.

[4] Shengju Z., Jiaosheng Z., Xiaoping A., et al., Oil production calculation for rhombic inverted nine-spot areal well pattern of low permeability reservoirs, Lithologic Reservoirs, 2012, 24(6), 115-120.

[5] Shucheng W., Ming L., Yunxian W., et al, Mass production optimization based on analysis of waterflood response, Xinjiang Petroleum Geology, 2010, 31(2), 178-180.

[6] Qing Y., Haiyang Y., Yefei W., et al., Technologies of in-depth profile control in China, Fault-Block Oil & Gas Field, 2009, 16(4), 68-71.

[7] Zhengming Y., Zhuangzhi M., Yutian L., et al., A Measured Method for In Situ Viscosity of Fluid in Porous Media by Nuclear Magnetic Resonance, Geofluids, 2018,9542152.

[8] Lu W., Yuedong Y., Shan H., et al., Transient cross flow law for fractured tight oil reservoirs, Fault-Block Oil & Gas Field, 2016, 23(3), 329-333.

[9] Dongfeng Z., Xinwei L., Dandan Y., et al., Discrimination of channeling of fractured reservoirs between wells based on Extension theory, Petroleum Geology and Recovery Efficiency, 2013, 20(4), 65-68.

[10] Rui S., Mengmeng C., Jianjun L., et al., A Pore-Scale Simulation on Thermal-Hydromechanical Coupling Mechanism of Rock, Geofluids, 2017(21), 7510527.

[11] Zhao H., Meiqin L., Zhaoxia D., et al., Study of deep profile control and oil displacement technologies with nanoscale polymer microspheres, J. Colloid Interface Sci., 2014, 424(424), 67-74.

[12] Rongze Y., Yanan B., Kaijun W., et al., Numerical simulation study on diamond-shape inverted nine-spot well pattern, Physics Procedia, 2012, 24(Part A), 390-396.

[13] Wei L., Xizhe L., Zhengming Y., et al., Construction of dual pore 3-D digital cores with a hybrid method combined with physical experiment method and numerical reconstruction method, Transport in Porous Media, 2017, 120(1), 227-238.

[14] Feng X., Qinghui J., Mingxi C., Numerical Investigation on Hydraulic Properties of Artificial-Splitting Granite Fractures during Normal and Shear Deformations, Geofluids, 2018, 9036028.

[15] Rui S., Jianjun L., Mengmeng C., A new method to reconstruct structured mesh model from micro-computed tomography images of porous media and its application, Int. J. Heat Mass Transfer, 2017, 109, 705-715.

[16] Rui S., Mengmeng C., Jianjun L., Single and multiple objective optimization of a natural gas liquefaction processs, Energy, 2017, 124, 19-28.

[17] Rui S., Mengmeng C., Molecular simulation on competitive adsorption mechanism of CH_4/CO_2 on shale kerogen, Arabian J. Geosciences, 2018, 11, 403.

[18] Quanhua H., Yun L., Chong C., Prediction of water breakthrough time for bottom-water gas reservoir with barrier, Lithologic Reservoirs, 2016, 28(4), 82-87.

[19] Gang H., A new method for calculating volumetric sweep efficiency in a water-flooding oilfield, Petrol. Explor. Development, 2013, 40(1), 103-106.

[20] Jian X., Xiangjun L., Zhen C., Dynamic productivity prediction model for fracturing wells in low permeability gas reservoir, Lithologic Reservoirs, 2013, 25(2), 82-85.

[21] Lin Y., Xiaoping L., Jianjun L., Productivity calculation method of fractured horizontal wells with gas-water two-phase in low permeability gas reservoirs, Lithologic Reservoirs, 2016, 28 (4), 88-94.

[22] Richard A.D., Yuping Z., Mechanistic study of the selective action of oil and water penetrating into a gel emplaced in a porous medium, J. Petrol. Sci. Eng., 1994, 12(2), 113-125.

[23] Jenn-Tai L., Haiwang S., Seright R.S., Why do gels reduce water permeability more than oil permeability?, SPE Reservoir Eng., 1995, 10(4), 282-286.

[24] Seright R.S., Reduction of gas and water permeabilities using gels, SPE Production & Facilities, 1995, 10(2), 103-108.

[25] Zhaoqi F., Linsong C., Xiaorong L., et al., Influence factor analysis and field application of deep profile-controlling based on the streamline model, Journal of Southwest Petroleum Univer-

sity (Science & Technology Edition) , 2013, 35(2), 121-126.
[26] Xiaorong L., Yuqin J., Zhaoqi F., et al., Effectiveness evaluation and streamline field analysis of polymer microspheres profile-controlling in fractured reservoirs, J. Oil Gas Techn., 2012, 34(7), 125-128.
[27] Islam M.R., Farouq Ali S.M., Numerical simulation of foam flow in porous media, J. Canad. Petrol. Techn., 1990, 29(4), 47-51.
[28] Rossen W.R., Mamun C.K., Minimal path for transport in networks, Phys. Rev. B Condens. Matter, 1993, 47(47), 11815-11825.
[29] Balan H.O., Balhoff M.T., Nguyen Q.P., et al., Network modeling of gas trapping and mobility in foam enhanced oil recovery, Energy & Fuels, 2011, 25(9), 3974-3987.
[30] Zitha P.L.J., Du D.X., A new stochastic bubble population model for foam flow in porous media, Transport in Porous Media, 2010, 83(3), 603-621.
[31] Zanganeh M.N., Kam S.I., Laforce, T., et al., The method of characteristics applied to oil displacement by foam, SPE Journal, 2009, 16(1), 8-23.
[32] Hamouda A.A., Gupta S., Enhancing Oil Recovery from Chalk Reservoirs by a Low-Salinity Water Flooding Mechanism and Fluid/Rock Interactions, Energies, 2017, 10(4), 576.
[33] Juan W., Shuoliang W., Wei L., et al., Formula optimization and rheology study of clean fracturing fluid, J. Mol. Liquids, 2017, 241, 563-569.
[34] Wei L., Zhengming Y., Juan W., et al., Wormlike micelles with pH-induced rheological property formed by cationic surfactant/anthranilic acid mixed aqueous solution, J. Mol. Liquids, 2016, 224 (Part A), 333-337.
[35] Zhao H., Meiqin L., Zhaoxia D., et al., Study of deep profile control and oil displacement technologies with nanoscale polymer microspheres, J. Colloid Interface Sci., 2014,424(15),67-74.
[36] Amaziane B., Jurak M., Keko A.Ž, Modeling compositional compressible two-phase flow in porous media by the concept of the global pressure, Comput. Geosci., 2014,18(3-4), 297-309.
[37] Andreolli I., Zortea M., Baliño J.L., Modeling offshore steady flow field data using drift-flux and black-oil models, J. Petrol. Sci. Eng., 2017, 157, 14-26.